Clinical Studies

Cancer Research

Functionally Null *RAD51D* Missense Mutation Associates Strongly with Ovarian Carcinoma

Barbara Rivera[1,2], Massimo Di Iorio[1], Jessica Frankum[3], Javad Nadaf[1,4], Somayyeh Fahiminiya[5], Suzanna L. Arcand[5], David L. Burk[6], Damien Grapton[2], Eva Tomiak[7], Valerie Hastings[7], Nancy Hamel[5], Rabea Wagener[8], Olga Aleynikova[9], Sylvie Giroux[10], Fadi F. Hamdan[11], Alexandre Dionne-Laporte[12], George Zogopoulos[5,13], Francois Rousseau[10], Albert M. Berghuis[14], Diane Provencher[15], Guy A. Rouleau[12], Jacques L. Michaud[11], Anne-Marie Mes-Masson[15], Jacek Majewski[1,4], Susanne Bens[8], Reiner Siebert[8], Steven A. Narod[16,17], Mohammad R. Akbari[16,17], Christopher J. Lord[3], Patricia N. Tonin[1,5,18], Alexandre Orthwein[2,19], and William D. Foulkes[1,2,5,20]

Abstract

RAD51D is a key player in DNA repair by homologous recombination (HR), and *RAD51D* truncating variant carriers have an increased risk for ovarian cancer. However, the contribution of nontruncating *RAD51D* variants to cancer predisposition remains uncertain. Using deep sequencing and case–control genotyping studies, we show that in French Canadians, the missense *RAD51D* variant c.620C>T;p.S207L is highly prevalent and is associated with a significantly increased risk for ovarian high-grade serous carcinoma (HGSC; 3.8% cases vs. 0.2% controls). The frequency of the p.S207L variant did not significantly differ from that of controls in breast, endometrial, pancreas, or colorectal adenocarcinomas. Functionally, we show that this mutation impairs HR by disrupting the RAD51D–XRCC2 interaction and confers PARP inhibitor sensitivity. These results highlight the importance of a functional RAD51D–XRCC2 interaction to promote HR and prevent the development of HGSC. This study identifies c.620C>T;p.S207L as the first bona fide pathogenic *RAD51D* missense cancer susceptibility allele and supports the use of targeted PARP-inhibitor therapies in ovarian cancer patients carrying deleterious missense *RAD51D* variants. *Cancer Res; 77(16); 4517–29. ©2017 AACR.*

Introduction

Ovarian cancer is the second most common gynecologic malignancy in developed countries and has the highest morbidity and mortality rates among cancers of the reproductive system. Approximately 20% of all ovarian cancer cases are associated with pathogenic germline variants in cancer susceptibility genes (1). Disease-causing variants in hereditary breast and ovarian cancer (HBOC) occur most frequently in *BRCA1* and *BRCA2*, which encode key players in the repair of DNA double-strand breaks (DSB) by homologous recombination (HR). Three HR proteins belonging to the RAD51 paralog complex (RAD51B, RAD51C, and RAD51D) have been associated with HBOC (2), while the role of two others (XRCC2 and XRCC3) remains unclear. RAD51 is a RecA-like DNA recombinase that catalyzes strand invasion and strand exchange between homologous sequences during HR-mediated DSB repair. This process is facilitated by the recruitment of RAD51 paralogs that form two distinct complexes in human cells: the CX3 dimer, consisting of RAD51C and XRCC3, and a larger BCDX2 complex composed of RAD51B, RAD51C, RAD51D, and XRCC2. Importantly, RAD51 paralog deficiency results in reduced RAD51 recruitment to DSBs, impaired HR and hypersensitivity to both DNA cross-linking agents, and ionizing radiation. Germline truncating variants in *RAD51D* have been reported to predispose to ovarian cancer and to result in susceptibility to PARP inhibitors (3).

Following the discovery of an association between RAD51D mutations and ovarian high grade serous carcinoma (HGSC), other truncating mutations and some missense variants of unknown

[1]Department of Human Genetics, McGill University, Montreal, Canada. [2]Lady Davis Institute, Montreal, Canada. [3]The CRUK Gene Function Laboratory and Breast Cancer Now Toby Robins Research Centre, The Institute of Cancer Research, London, United Kingdom. [4]Genome Quebec Innovation Centre, Montreal, Canada. [5]Cancer Research Program, The Research Institute of the McGill University Health Centre, Montreal, Canada. [6]Department of Biochemistry, McGill University, Montreal, Canada. [7]Department of Genetics, University of Ottawa, Children's Hospital of Eastern Ontario, Canada. [8]Institute of Human Genetics, University of Ulm and University of Ulm Medical Center, Ulm, Germany. [9]Department of pathology, Jewish General Hospital, Montreal, Canada. [10]University of Laval and CHU Research Centre, Quebec; Canada. [11]CHU Sainte-Justine Research Center, Montreal, Canada. [12]Montreal Neurological Institute, McGill University, Montreal, Canada. [13]The Goodman Cancer Research Centre, McGill University, Montreal, Canada. [14]Department of Biochemistry, McGill University, Montreal, Canada. [15]Centre de recherche du CHUM and Institut du cancer de Montréal, University of Montreal, Montreal, Canada. [16]Dalla Lana School of Public Health, Toronto, Canada. [17]Women's College Hospital, Toronto, Canada. [18]Department of Medicine, McGill University, Montreal, Canada. [19]Department of Oncology, McGill University, Montreal, Canada. [20]Department of Medical Genetics, Research Institute, McGill University Health Centre, Montreal, Canada.

Note: Supplementary data for this article are available at Cancer Research Online (http://cancerres.aacrjournals.org/).

M. Di Iorio, J. Frankum, and J. Nadaf contributed equally to this article.

Current address for J. Nadaf: St Jude Children's Research Hospital (SJCRH), Memphis, TN.

Corresponding Author: William D. Foulkes, Cancer Research Program, McGill University Health Centre, 1001 Boul Décarie, Montreal, Quebec H4A 3J1, Canada. Phone: 514-412-4427; Fax: 514-412-4296; E-mail: william.foulkes@mcgill.ca

doi: 10.1158/0008-5472.CAN-17-0190

significance have been described (4, 5). Recently, an association between *RAD51D* variants that are predicted to truncate the protein with high-grade serous carcinoma (HGSC) has been postulated (6). In monoallelic diseases, as well as in complex traits, it has been proposed that a percentage of the missing heritability is due to rare variants conferring high-to-moderate risk of the disease (7). Understanding the clinical significance of rare nontruncating variants constitutes a necessary but challenging task, particularly in novel genes such as *RAD51D* where the incidence and penetrance of disease-associated alleles are not yet established (8).

Most studies base variant classification on multifactorial likelihood models of pathogenicity easy to integrate in a high-throughput screening pipeline (9). In contrast, characterization of a variant's functional effects involves lengthy, comprehensive analyses frequently limited to variants located in genes and domains with established functions (10–12). No pathogenic missense variants have thus far been confirmed in *RAD51D*.

Assessing the pathogenicity of rare variants is often difficult, but founder alleles within genetically homogenous populations can attain high enough frequencies to be detected in small series, enabling case–control studies to estimate cancer risk (13). Moreover, identifying founder mutations has important clinical implications for prevention and management of individuals at risk, making targeted screening programs and adapted surveillance plans feasible for carriers and their families.

We sought out to determine whether the c.620C>T missense variant was associated with risk for ovarian cancer through a multifaceted study, including a case–control, functional characterization of the effects of the variant in the DNA repair activity of RAD51D, and genomic profiling of RAD51D tumors.

Patients and Methods

Patients and samples

The study was approved by the Institutional Review Board of the Faculty of Medicine of McGill University (Montreal, Canada). Participants were recruited in compliance with the second edition of the Canadian Tri-Council Policy Statement of Ethical Conduct for Research Involving Humans and Eligible Persons or Designates and signed a consent form in accordance with the Institutional Review Board approvals.

Two independent families with three siblings affected with HGSC were referred to the cancer genetics clinic as part of the discovery phase of this study. For the validation phase, we studied a total of 2,416 cancer patients and a control group composed of 335 women and 595 men. Subjects are described in detail in the Study Population section of this article

Index family

The first family studied was referred to the Montreal General Hospital (Montreal, Canada) cancer genetic clinic in 2012. The proband and her two sisters were affected with HGSC and were of a French Canadian (FC) ethnicity (Fig. 1A–G). The proband was diagnosed with International Federation of Gynecology and Obstetrics (FIGO) stage IIIC HGSC of proposed primary peritoneal origin at age 77 years. Her sister was diagnosed at age 75 with a poorly differentiated adenocarcinoma of gynecologic, likely ovarian, origin. A second sister of the proband was diagnosed at age 76 with a stage IV high grade Müllerian carcinoma of the endometrium, of probable serous differentiation due to strong p53 staining, with two 2.5-mm foci of high-grade carcinoma on the surface and cortex of the left ovary (Fig. 1C). In all cases, treatment involved debulking surgery, followed by three cycles of neoadjuvant chemotherapy. Formalin-fixed paraffin-embedded (FFPE) tissue and blood from the three affected sisters in the index family were collected, including two primary tumor samples and one lymph node metastasis. Where blood or saliva were unavailable, germline DNA was obtained from FFPE sections of lymph nodes containing only normal tissue. A clinical testing gene panel was performed on the proband that identified a *RAD51D* c.620C>T;p.S207L variant.

Families 2, 3, and 4

In 2014, a second family of FC origin was referred to us in which the proband was diagnosed at age 59 with bilateral synchronous HGSC of the ovaries and fallopian tubes (Supplementary Fig. S1A). Two of her sisters were affected by ovarian cancer, diagnosed at ages 44 and 54, respectively. Their mother was diagnosed with breast cancer (lobular invasive carcinoma, grade II, stage T2N0Mx) at age 91. Clinical testing led to the identification of the same variant in *RAD51D*.

The third familial case was identified among our in-house exomes from a previous study involving 51 FC high-risk breast cancer cases (14). The proband had an invasive ductal carcinoma breast cancer diagnosed at 62, and serous peritoneal carcinoma diagnosed at age 72. Her daughter was diagnosed with an invasive ductal carcinoma and ductal carcinoma *in situ* at age 52. The proband's sister was also diagnosed with breast cancer and her father and a brother both had a history of cancer.

During the genotyping phase of this project, a fourth familial case was identified among the high-risk FC breast cancer cases, referred to as family 4 in this study. The proband had bilateral nonsynchronous breast cancer diagnosed at 35 and 54, as well as endometrial polyps and has a sister with breast cancer, and a strong family history for other malignancies.

Study population

We studied a total of 2,425 cancer patients, affected by one of five common epithelial cancer types. We included 341 DNA samples from patients with ovarian HGSC recruited from a major French-speaking hospital in Montreal, Centre Hospitalier de l'Université de Montréal (CHUM), Hôpital Notre-Dame, where at least 88% of patients are of FC ethnicity (15). Samples were derived from peripheral blood lymphocytes ($n = 312$), ovarian cancer specimens ($n = 28$), or malignant ascites ($n = 1$), all of them previously tested for at minimum the six most common BRCA1/2 FC founder mutations (15, 16).

Furthermore, we looked at 1,456 DNA samples derived from peripheral blood lymphocytes of breast cancer patients all previously tested for *BRCA1*, *BRCA2*, and *PALB2* founder mutations: 212 (207 women, 5 men) were high-risk cases selected on the basis of their familial and personal antecedents of HBOC and the age of diagnosis, and 1,235 (all women) were moderate risk either aged less than 50 years at diagnosis or who were 50 years or older and had at least two affected first- or second-degree relatives. The high-risk group contained probands from FC HBOC families ($n = 51$) recruited from multiple hospitals in Montreal between 1995 and 2013, who were subjected to whole-exome sequencing (WES; ref. 14); the rest were cases recruited from cancer clinics at the Montreal General Hospital ($n = 76$) and Jewish General Hospital ($n = 85$). For breast cancer cases recruited in English hospitals in Montreal, FC ethnicity was defined as at least three grandparents being FC. The moderate-risk cases were recruited at the Research

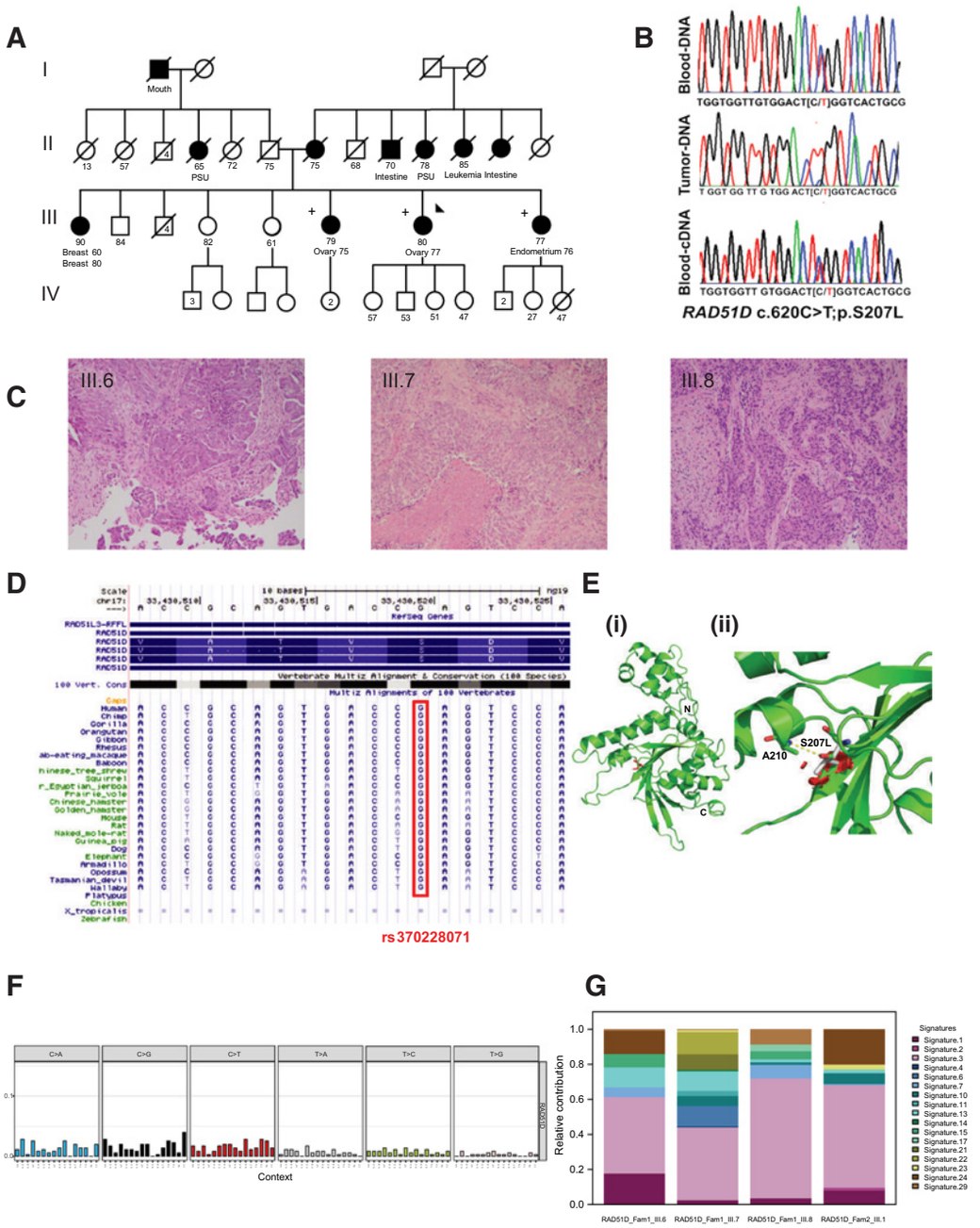

Figure 1.

A, Pedigree of family 1. +, carriers of c.620C>T;p.S207L; arrow, proband; ovary, ovarian HGSC; endometrium, endometrial cancer; breast, breast cancer. **B,** *RAD51D* sequence surrounding the c.620C>T;p.S207L mutation. Top, germline; middle, ovarian HGSC of the proband; bottom, cDNA from blood of the proband. **C,** H&E staining of tumors from affected sisters. Left, ovarian HGSC of the proband; middle, metastases of ovarian HGSC in III.6; right, endometrial cancer in III.8. Magnification, ×100. **D,** Conservation of c.620C>T;p.S207L across species. c.620C>T;p.S207L variant is highly conserved across species. **E,** RAD51D structural model. The p.S207L mutation site was generated on the basis of homology to archaeal RECA and yeast RAD51. This model shows the S207 residue positioned at the end of one of the strands of the central β-sheet, oriented so that it could form a hydrogen bond with the amide backbone group of the A210 residue and could help structure the Walker B motif. The introduction of a leucine residue at this position would abrogate this hydrogen bond and cause steric clashes with an adjacent β-strand, likely disrupting the structure of RAD51D Walker B motif and altering its activity during HR-mediated DSB repair. (**i**) A cartoon diagram of the RAD51D model, with the location of S207 shown as red sticks. (**ii**) A close-up view of the S207L mutation site. S207 and A210 are shown as green sticks, with their hydrogen bond interaction shown as a yellow dashed line. The superimposed S207L mutation is shown as gray sticks. Steric clashes with the adjacent β-strand are shown as red discs. **F,** Molecular signature from the 96 mutational profiles in RAD51D p.S207L tumors (individuals III.6, III.7, and III.8 from family 1 and individual III.1 from family 2). **G,** Contribution of the different molecular signatures to the RAD51D familial tumors.

Centre of CHUM, Hôpital Hôtel-Dieu in Montreal ($n = 1,235$), selected as per the criteria by Cybulski and colleagues (14). In addition, we screened a group of 107 DNA samples (41 women, 66 men) from unselected pancreatic adenocarcinoma patients diagnosed and/or treated at the McGill University Health Centre; 36 of them correspond to an extension of a cohort recruited at various Montreal hospitals between 1996 and 1998. FC ethnicity was defined as at least three grandparents being FC (17). The remaining 71 cases were recruited through the McGill University Health Centre cancer clinic following less stringent criteria, including individuals with at least 1 grandparent of an FC origin. Finally, we screened leukocyte-derived DNA samples from unselected endometrial cancer patients ($n = 367$) recruited at the CHUM-Hôpital Notre-Dame (Montreal, Canada). This series includes: endometrioid adenocarcinomas ($n = 260$), mixed cell adenocarcinoma ($n = 58$), serous cystoadenocarcinomas ($n = 23$), clear cell adenocarcinoma ($n = 10$), adenocarcinomas on adenomatous polyp ($n = 6$), mucinous adenocarcinoma ($n = 4$), adenocarcinoma on polyadenoma ($n = 2$), unspecified adenocarcinoma ($n = 2$), one undifferentiated carcinoma, and one epidermoid carcinoma. A series of DNA derived from FFPE normal DNA samples from 154 unselected colorectal carcinoma patients (66 women, 88 men) recruited at the Centre Hospitalier de l'Université Laval in Quebec was also included in the study (18). A baseline frequency for the variant of interest in this study, *RAD51D*:c.620C>T [p.S207L], was established in a group of 930 healthy FC controls comprised of unaffected individuals ($n = 335$ women and $n = 104$ men) recruited in-house at the Jewish General Hospital, Montreal General Hospital, and CHUM hospitals in Montreal, and a series of otherwise unaffected individuals ($n = 194$ women and $n = 297$ men) enrolled in WES studies of neurodevelopmental disorders at the CHU Saint-Justine in Montreal. For control individuals recruited in English hospitals in Montreal, FC ethnicity was defined as at least three grandparents being FC.

Nucleic acid isolation

For index family members, germline DNA was obtained from peripheral blood leukocytes, saliva, or FFPE tissue samples of unaffected lymph nodes. Tumor DNA was obtained from FFPE tumor samples. The Gentra Puregene Blood Kit (Qiagen) was used to perform saliva and leukocyte DNA extractions. All DNA obtained from FFPE was extracted from cells macrodissected from 10 μm unstained serial tissue sections following pathology revision to enrich separately for tumor and normal areas. DNA was subsequently isolated using the QIAamp DNA FFPE Tissue Kit (Qiagen). Where possible, RNA was extracted from patient leukocytes using the RecoverAll Total Nucleic Acid Isolation Kit (Ambion) and reverse transcribed into cDNA using SuperScriptIII first-strand cDNA synthesis (Thermo Fisher Scientific).

mRNA analysis

RAD51D transcript NM_002878 was used to design cDNA-specific PCR primers for the p.S207L mutation. Presence of the modified transcript in blood leukocyte–derived cDNA was verified using PCR followed by Sanger sequencing. Primers are available upon request.

Genotyping

Genotypes at the *RAD51D* variant locus from 51 high-risk breast cancer samples were obtained from existing WES data (14). The remaining high-risk breast cancer, endometrial, and pancreas cancer samples as well as the in-house controls were genotyped using a high-resolution melting (HRM) assay. Primers are available upon request. Genotyping of moderate-risk breast cancer samples and the ovarian HGSC samples employed a custom TaqMan SNP Genotyping assay. The primer and reporter sequences are available upon request. The assays were performed as described previously (19). Colorectal carcinoma samples were genotyped by Sanger sequencing. Samples presenting abnormal patterns by HRM or TaqMan as well as samples where WES data revealed the presence of c.620C>T variant were further validated by Sanger sequencing, which was performed using the 3730XL DNA Analyzer system (Applied Biosystems, Thermo Fisher Scientific) at the McGill University and Genome Quebec Innovation Center (MUGQIC; Montreal, Quebec, Canada). Primers are available upon request. Chromatograms were compared with the NCBI reference sequence (RefSeq) reported in GenBank NM_002878.3 and the genomic structures available from the February 2009 GRCh37/hg19 assembly of the human reference genome.

Haplotyping

Polymorphic microsatellite repeat markers D17S2129, D17S1872, D17S933, D17S1846, D17S907, and the *RAD51D* c.620C>T;p.S207L variant locus were used for haplotype analysis (Supplementary Table S1) as described by Rudkin and colleagues (20).

Tumor profiling and WES

WES. Tumor and normal DNA of all three sisters (III.6, III.7, and III.8) from the index family (Fig. 1A), as well as DNA from the proband (III.1) from the second family (Supplementary Fig. S1A), were subjected to WES. WES was performed at the McGill University and Génome Québec Innovation Centre (MUGQIC). Six FFPE-derived DNA samples (~100 ng) and two blood/saliva-derived samples (~500 ng) underwent exome capture (Nextera Rapid Capture Exome Kit), followed by 100-bp paired-end sequencing on Illumina HiSeq 2000.

Bioinformatics analysis of exome sequencing data was performed as described previously (21) In brief, reads were aligned to UCSC hg19 reference genome with Burrows–Wheeler aligner (bwa mem version 0.7.7) The genome analysis toolkit (GATK) was used to assess coverage of consensus coding sequence sites and to perform local realignment of reads around small insertions and deletions (indel; ref. 22). PCR duplicate reads were marked using Picard (http://picard.sourceforge.net/). Germline variants were called using SAMtools (version 1.8) and somatic single-nucleotide variants (SNV) and indels were called using Mutect (see https://confluence.broadinstitute.org/display/CGA Tools/MuTect for method) and IndelLocator (for method see https://confluence.broadinstitute.org/display/CGATools/Indelocator), respectively. The list of variants was then subjected to several filtering steps, and variants were filtered out if they fulfilled any one of the following criteria: (i) genomic position of variant covered by <10×; (ii) <5 reads support the alternative variant; (iii) variant has allelic ratio <5% for SNVs or <15% for indels; (iv) variant has allele frequency >0.001 in our noncancer (~2,000 exomes sequenced previously in our center) or ExAC databases; or (v) variant seen as homozygote in ExAC database. Finally, the remaining variants were annotated by ANNOVAR (23), and only the most likely damaging variants (nonsense, canonical

splice-site, and missense variants, and coding indels) predicted to be deleterious by at least 3 of 5 bioinformatics algorithms (SIFT, PolyPhen, MutationTaster, Revel, and MCAP) were considered for further analysis. The Integrative Genomics Viewer (24) was used for the manual examination and visualization of all potential candidate variants. To investigate the presence of any somatic mutations in DNA repair genes, we cross-referenced our list of variants with 193 DNA repair genes reported in the recent publication by Chae and colleagues (25) and presented the results in Supplementary Table S2.

ExomeAI was used to perform allelic imbalance analysis as described previously (26) In brief, ExomeAI detects allelic imbalance events across samples using all heterozygous variants (BAF values of 0.05–0.95). Then, CBS algorithm was used to segment the variants into similar BAF values. Significance of each segment was evaluated using different statistical tests and a large internal WES control dataset (see more details in ref. 26). Somatic mutation signature analysis was performed on all synonymous and nonsynonymous somatic mutations that passed the aforementioned filtering steps using SomaticSignatures, a Bioconductor package. Briefly, 96 trinucleotides mutational context [A|C|G|T] [C>A|C>G|C>T|T>A|T>C|T>G] [A|C|G|T] were extracted and compared with the current known set of mutational signatures listed by the Sanger Institute (27).

Loss-of-heterozygosity analysis. WES data were employed to interrogate the presence of loss-of-heterozygosity (LOH) in the tumors of affected cases from family 1 and 2. LOH in available tumors from the unselected ovarian HGSC cohort was validated by Sanger sequencing. Primers are available upon request.

TP53 somatic mutation screening for HGSC cancer cases. Tumor DNA samples from cases that tested positive for the *RAD51D*-p.S207Lvariant allele were also screened for somatic *TP53* mutations in protein-coding exons 2 to 11 and adjacent splice sites. Mutation analysis was performed as described previously (28). Sequence chromatograms were compared with NCBI reference sequence (RefSeq) reported in GenBank NM_000546.5 (TP53) and the genomic structures available from the February 2009 GRCh37/hg19 assembly of the human reference genome. Sequence variants were compared with those reported in the SNP Database (www.ncbi.nlm.nih.gov/SNP). In addition, variants were evaluated on the basis of information in the International Agency for Research on Cancer (IARC) TP53 Database (www-p53.iarc.fr).

FISH. FISH analyses were performed on sections from FFPE tissues using analogous protocols to those described by Ventura and colleagues (29). The *RAD51D* locus was investigated with a FISH probe (BAC RP11-294G4, obtained from Life Technologies) spanning the *RAD51D* gene. Centromeric probes for chromosomes 10 and 17 (Abbott) served as internal controls. Extraction and labeling of BAC DNA, preparation of slides, and hybridizations were conducted according to standard procedures. Slides were evaluated using Zeiss fluorescence microscopes equipped with appropriate filter sets. Digital image acquisition and processing were performed using the ISIS digital image analysis system (MetaSystems).

In silico modeling

The RAD51D sequence was submitted to the Phyre2 modeling web portal (30). The software was able to model 96% of the RAD51D structure at >90% confidence based on the coordinates of three archaeal RECA and two yeast RAD51 template structures (PDB ID: 1pzn, 3lda, 1t4g, 2dfl, and 1szp). The molecular graphics program PyMOL was used to visualize the model, examine the consequences of introducing the p.S207L mutation, and to produce figures (31).

SNP arrays

FFPE-derived DNA samples of five tumor samples corresponding to probands III.6 (two samples from different tumor blocks), III.7, and III.8 of family 1 and III.1 of family 2 were hybridized on an OncoScan Array (Affymetrix) for copy number analyses. Arrays were normalized using the OncoScan Console 1.3 Software from Affymetrix and analyzed using the Nexus Express software (BioDiscovery).

Cell lines

The CHO-RAD51D.1 cells were obtained from Dr. Larry Thompson (Lawrence Livermore National Laboratory, Livermore, CA). They were last tested for mycoplasma contamination in October 5, 2015. Cells were thawed and passaged twice before transfection. Consecutively, they were cultured in selection media for a week and expanded until enough cells were available to perform drug sensitivity assays. The U2OS DR-GFP cells were a gift from the laboratory of Dr. Jeremy Stark (Beckman Research Institute of the City of Hope, Duarte, CA). HEK293T cells were purchased from ATCC. The parental cell lines were tested for mycoplasma contamination in July 2016 using the PCR Mycoplasma Detection Kit from abmGood. All cell lines were authenticated by STR DNA profiling. They were passaged once before the start of the experiments.

Plasmids and construct

A CHO-RAD51D–deficient cell line (RAD51D.1; a gift from Dr. Thompson's laboratory to C.J. Lord; ref. 32) was used to stably express the c.620C>T;p.S207L variant (RAD51D.1-p.S207L), or wild-type RAD51D (RAD51D.1-wt); a proficient RAD51D.3 cell line was used as a control.

The gRNAs targeting the LMNA locus and the mClover-tagged LMNA are described in the work of Pinder and colleagues, 2014 (33). The complementary DNA of *RAD51D* was obtained from the MGC premier human ORFeome Complete Library (Transomic) through the McGill Genetic Perturbation Service. It was subcloned into the pDEST-pcDNA5-Flag-Nterm vector (a gift from A.-C. Gingras, Lunenfeld-Tanenbaum Research Institute; Mount Sinai Hospital, Toronto, Ontario), the pDEST-pcDNA5-mCherry vector (a gift from A.-C. Gingras) or the pDEST-LacR vector (a gift from D. Durocher, Lunenfeld-Tanenbaum Research Institute; Mount Sinai Hospital, Toronto, Ontario) using Gateway cloning technology (Thermo Fisher Technology). Point mutations and siRNA-resistant versions of RAD51D constructs were generated using the QuikChange Site-Directed Mutagenesis Kit (Agilent).

RNAi

All siRNAs employed in this study were single duplex siRNAs purchased from Dharmacon. RNAi transfections were performed using Lipofectamine RNAiMax (Invitrogen) in a forward transfection mode. The individual siRNA duplexes were *RAD51D* (J-017467-07-0002), *RAD51* (M-003530-04), *CtIP*/*RBBP8* (M-001376-00), and nontargeting control siRNA (D-001210-02). siRNAs were transfected 72 hours before cell processing.

RAD51 foci induction and immunofluorescence staining

RAD51 and γ-H2AX foci detection were assessed by inducing DSBs through neocarzinostatin treatment in parallel for RAD51D.1-p.S207L, RAD51D.D1-wt, RAD51D.1 and RAD51D.3. Cells were seeded in chamber slides and treated with 100 ng/mL neocarzinostatin for three hours. Immunofluorescence was performed as previously published by Orthwein and colleagues (34).

HR-based repair assay

The efficiency of HR was assessed using an I-SceI repair substrate (DR-GFP) integrated in the HeLa cell line. HeLa DR-GFP cells were treated with the indicated siRNAs, and cells were transfected with a plasmid expressing I-SceI and the indicated siRNA-resistant mCherry-tagged construct using Lipofectamine 2000 (Thermo Fisher Scientific) 24 hours later. Forty-eight hours after I-SceI transfection, cells were trypsinized and the percentage of GFP/mCherry-positive cells was determined by flow cytometry.

The efficiency of HR was also assessed using a CRISPR/Cas9–mediated gene-targeting assay. Chinese hamster ovary (CHO) cells expressing the different RAD51D mutants were trypsinized, washed with PBS, and electroporated with 1.25 μg of sgRNA plasmid and 1.25 μg of donor template using the 4-D Nucleofector system (Lonza; protocol 111). Cells were plated in medium and grown for 72 hours before flow cytometry analysis as described previously (34).

RAD51D–XRCC2 coimmunoprecipitation

HEK293T cells were transiently transfected with the indicated Flag-tagged RAD51D constructs as indicated above. Forty-eight hours posttransfection, cells were collected by trypsinization, washed once with PBS, and lysed in 500 μL of lysis buffer [20 mmol/L Tris-HCl pH 8.0, 300 mmol/L NaCl, 1% Triton X-100, 2 mmol/L EDTA, and complete protease inhibitor cocktail (Roche)] on ice. Lysates were centrifuged at 15,000 × *g* for 10 minutes at 4°C, and protein concentration was evaluated using absorbance at 280 nm. Equivalent amounts of proteins (0.5–1 mg) were incubated with 30 μL of M2 anti-Flag beads (Sigma) for 2 hours at 4°C. Beads were collected by centrifugation, washed once with lysis buffer and twice with TBS, and eluted by boiling with 2× Laemmli buffer, before analysis by SDS-PAGE and immunoblotting.

RAD51D–XRCC2 quantification

U2OS LacO cells were plated on glass coverslips and transiently transfected with the indicated LacR-tagged RAD51D constructs as indicated above. Forty-eight hours posttransfection, cells were fixed with 2% (w/v) paraformaldehyde in PBS for 20 minutes at room temperature, permeabilized with 0.3% (v/v) Triton X-100 for 20 min at room temperature, and blocked with 5% BSA in PBS for 30 minutes at room temperature. Cells were subsequently incubated with an anti-XRCC2 antibody (Santa Cruz Biotechnology, sc-365854) diluted in PBS-BSA for 2 hours at room temperature (1:100). Cells were next washed with PBS and then incubated with an anti-mouse Alexa 488 antibody diluted in PBS-BSA (1:500) supplemented with 0.8 μg/mL of DAPI to stain DNA for 1 hour at room temperature. The coverslips were mounted on glass slides with Prolong Gold mounting agent (Invitrogen). Visualization method is detailed in the section below.

LSM confocal microscopy

Imaging work was performed at the Lady Davis Research Institute Cell Imaging Facility. Images were collected using a Zeiss Axiovert 200M inverted microscope equipped with the LSM 5 Pascal point laser module, the LSM AIM acquisition software, and 2 PMT detectors for spectral detection. Quantification was performed using ImageJ software.

Cell survival assay

Stable cell lines expressing the RAD51D c.620C>T, c.47TC;p.M16T, wild-type (wt), and empty constructs were produced in a RAD51D-deficient cell line (CHO RAD51D.1). In parallel, an empty construct was produced in the RAD51D wt cell line (RAD51D.3). Human RAD51D was expressed via a C-terminal Flag epitope–tagged cDNA. Reexpression of the RAD51D constructs was tested by Western blot analysis.

PARP inhibitor sensitivity was tested by 96-well survival assays using olaparib and talazoparib (BMN 673) as described previously (3). Cisplatin sensitivity was measured as a control.

Antibodies

We employed the following antibodies: anti-tubulin (CS3873, Cell Signaling Technology), rabbit anti-RAD51D (EPR16205 ab202063, Abcam), and rabbit anti-RAD51 (#70-001, BioAcademia) were used to check siRNA efficiency. Mouse anti-XRCC2 (sc-365854, Santa Cruz Biotechnology) and mouse anti-Flag (clone M2, Sigma) were used for the coimmunoprecipitation blots. Rabbit anti-RAD51 (#70-001, BioAcademia) and anti-mouse γ-H2AX (05-636 EMD Millipore) were used for immunofluorescence in the foci induction. Mouse anti-Flag (clone M2, Sigma) and anti-Actin Santa Cruz Biotechnology I-19 (sc-1616) antibodies were used to test stable expression or RAD15D constructs in the transfected CHO-RAD51D cells lines. Secondary antibodies: anti-mouse-HRP Cell Signaling Technology (CS7076), anti-rabbit-HRP Cell Signaling Technology (CS7074). Anti-mouse-Alexa 488 and anti-rabbit-Alexa647 from Thermo Fisher Scientific were used in immunofluorescence staining.

Statistical analyses

Two-sided Fisher exact test was used to compare the frequency of c.620C>T carriers in the cancer cases and controls. The 95% confidence intervals of proportions were calculated using the Wald method. ANOVA followed by Tukey test was used to compare the effects of the expression of p.S207L mutant with the RAD51D KO, RAD51D WT, and RAD51D cell lines in the RAD51 foci induction, HR-based repair assay (mClover), and RAD51D–XRCC2 *in vivo* quantifications (including the p.E233G and p.S207L + p.E233G mutants for this specific experiments).

ANOVA followed by Tukey test was used to compare the effects of the expression of p.S207L mutant with p.E233G, p.S207L + p.E233G, p.D206A, RAD51D WT, and RAD51D null cell lines in the DR-GFP–based repair assay.

Two-way ANOVA followed by Tukey test was used to compare the effects of the expression of p.S207L mutant with the RAD51D KO, RAD51D WT, p.M16T, and RAD51D cell lines in the cell survival assays.

Results

A woman presented to the Hereditary Cancer Clinic of the McGill University Health Centre with a personal and familial history of HGSC arising in the gynecologic tract (Fig. 1A). *BRCA1*/

2 testing revealed no deleterious variants. Further genetic testing identified the *RAD51D* c.620C>T;pS207L (rs370228071) (chr17: 33430520G>A (GRCh37): NM_002878.3) variant. Segregation analyses confirmed the presence of the variant in her two sisters, affected by HGSC of the ovary and endometrium, respectively (Fig. 1A–C). Sanger sequencing of the proband's cDNA from peripheral blood showed the variant is expressed (Fig. 1B). A second kindred referred to us for evaluation counted three women diagnosed with ovarian HGSC. All three were carriers of the c.620C>T variant (Supplementary Fig. S1A). The FC origin of both families suggested a possible founder variant. However, c.620C>T;pS207L was also previously described in two patients affected with ovarian HGSC (3, 5) and is a rare variant with an allele frequency of 3.3×10^{-5} in the ExAC database (35).

RAD51D c.620C>T;pS207L is associated with HGSC of the ovary in the FC population of Quebec

We performed a case–control study (Table 1) including persons affected by common epithelial cancers. This included ovarian HGSC, $n = 341$ (average age at diagnosis; range in years = 62; 36–87); endometrial cancer, $n = 367$ (average age, 62; 21–92); pancreas cancer, $n = 107$ (64; 31–81); colorectal cancer, $n = 154$ (67; 35–92); high-risk breast cancer cases, $n = 212$ (45; 19–73); and a series of moderate-risk breast cancer cases, $n = 1{,}235$ (48; 25–68) as well as 930 controls (529 women, 401 men, subject details provided in the Supplementary Material). The c.620C>T;pS207L variant was present in 13 of 341 (3.81%) of ovarian cancer cases and in 2 of 930 (0.22%) male and female controls ($P = 2 \times 10^{-6}$; Fisher exact test). Both carriers were males; no carriers were found among 529 females, 300 of which were frequency matched on age to the ovarian cancer HGSC series (mean age at testing for these 300 controls: 60.5 years; range, 36–79). We observed the variant in 6 of 1,447 breast cancer cases; no carriers were found among the endometrial, pancreas, or colorectal cancer cases.

The c.620C>T variant was not associated with a significantly increased risk of breast cancer ($P = 0.49$). Two carriers were identified in the high-risk breast cancer series (families 3 and 4, Supplementary Fig. S1B and S1C). The proband of family 3 developed a peritoneal HGSC 10 years after the diagnosis of a triple-negative breast cancer (TNBC). The family 4 proband was affected with bilateral breast cancer (one a TNBC) and disclosed familial antecedents of cancer, but HGSC was not reported in the family. Four additional carriers were found among a moderate-risk breast cancer series; none had familial or personal history of HGSC, one was a confirmed TNBC, two were estrogen receptors/progesterone receptors (ER/PR) positive, and the last was ER/PR negative with unknown HER2 status. Although we found no significant evidence for a relationship with breast cancer, some uncertainty remains whether TNBC risk could be related to this *RAD51D* variant.

The *RAD51D* c.620C>T;p.S207L variant segregates with HGSC phenotypes in families 1, 2, and 3 (Fig. 1A; Supplementary Fig. S1A–S1C). All c.620C>T carriers were negative for *BRCA1* and *BRCA2* FC founder mutations (mutation screening detailed in the Supplementary Material). Another *RAD51D* missense variant, c.698A>G p.E233G (rs28363284), cosegregated with c.620C>T in all carriers. It has a frequency of 0.017 among the European population in EXaC and was present in 27 of 645 (4.19%) controls tested, suggesting that c.620C>T arose on a chromosome carrying c.698A>G;p.E233G (Supplementary Fig. S2). Presence of a common founder haplotype spanning at least 669 kb was confirmed by genotyping 5 single tandem repeat markers flanking *RAD51D* in 29 carriers (Supplementary Table S1).

Tumor profiling of *RAD51D* c.620C>T;p.S207L carriers

WES of tumors from the three affected in family 1 and the proband of family 2 identified no intraexonic somatic mutations in *RAD51D*. However, ExomeAI (26) analysis of whole-exome data from all tumors revealed large segments of chromosome 17 exhibiting allelic imbalance, including the *RAD51D* locus, which could be due to copy number variants of the gene locus or copy-neutral loss of heterozygosity. Combined array and FISH analyses showed in all analyzed tumor samples from family 1 were remarkably complex with aberrant patterns of multiple gains, losses, and copy neutral losses of heterozygosity, which in all instances seem to be derived from a nondiploid (hyperploid) clone (Supplementary Fig. S3). Nevertheless, in all samples from this family, the changes resulted in an allelic imbalance at the *RAD51D* locus in line with the sequencing results. Results from genome-wide copy number analysis were less complex for the tumor sample of III.I in family 2, indicating two copies for *RAD51D* and the control probes (Supplementary Fig. S3). In all four tumor samples, the sequence data showed allelic imbalance, leading to an increase in ratio of RAD51D c.620T-(mutant) to c.620C-WT (Fig. 1B), ranging from 0.74 to 0.93 (where 0.5 represents a balanced allele ratio; data not shown).

Table 1. Frequency of RAD51D c.620C>T;p.S207L in cases and controls tested

	Common carcinomas ($n = 2{,}416$)						Controls ($n = 930$)		
	EC	PC	CRC	BC high risk	BC moderate risk	OC (HGSC)	Female (frequency matched to OC[a])	Female	Male
N (% FC)[b]	367 (100)	107 (100)	154 (97)	212 (100)	1,235 (100)	341 (88)	300 (100)	229 (100)	401 (100)
(n = women)	367	41	66	207	1,235	341			
S207L	0	0	0	2	4	13[c]	0	0	2
(%)	0	0	0	0.9	0.32	3.81	0	0	0.5
CI (95%)	—	—	—	0.03–3.60	0.09–0.86	2.18–6.47	—		0.01–1.92
Comparison *P* value	—	—	—	0.3	0.71	2×10^{-6}	—	—	—

NOTE: All *RAD51D* p.S207L carriers were negative for at least the 6 most common BRCA1 and BRCA2 FC founder mutations. *P* value, two-sided Fisher exact test representing the comparison of carriers among each series of cases and the total control group ($n = 930$).

Abbreviations: BC, breast cancer; CI, confidence interval of proportions expressed in percentage; EC, endometrial cancer; OC, ovarian cancer; PC, pancreas cancer.

[a]Women controls frequency age-matched to the ovarian cancer HGSC series (average age at testing 60.5; 36–79).

[b]Minimum percentage of individuals with an FC ancestry.

[c]Two of the 13 carriers had a personal history of breast cancer.

TP53 was the only somatically mutated gene common to all four tumors sequenced. The list of somatic mutations in DNA repair genes after filtering is detailed in Supplementary Table S2. Loss of heterozygosity at the *RAD51D*- c.620C>T locus was confirmed in all 10 unselected ovarian HGSC from which DNA was available. *TP53* somatic mutations were identified in all of them (Supplementary Table S3).

To further characterize the molecular profile of *RAD51D*-associated tumors, we studied their mutational signature profile, defined by the catalog of somatic mutations that reflect the biological processes driving the tumor (36). RAD51D-associated tumors showed clear predominance of signature 3 according to the numbering system described in ref. 36, as well as a high rate of copy number variants, both characteristic features of HR-deficient tumors (Fig. 1F and G; Supplementary Fig. S3).

Structural impact of the RAD51D p.S207L mutation

RAD51D is an ATPase whose structure is not yet completely understood. The N-terminal domain of the protein is known to be required for ssDNA binding. The ATPase domain includes the conserved ATP binding Walker A and B motifs that are crucial for its role in HR. Moreover, these motifs are implicated in binding to RAD51C and XRCC2, respectively, while residues 60–78 constitute the Linker domain that dictates proper interaction with RAD51C and XRCC2 (Supplementary Fig. S2). The p.S207L mutation is located directly in the Walker B motif, highly conserved throughout evolution (Fig. 1D). A 3D model of RAD51D is presented in Fig. 1E.

Abrogation of DNA damage foci formation in RAD51D-p.S207L mutants

RAD51D facilitates the accumulation of RAD51 to DSBs. Therefore, we tested whether RAD51p.S207L impacts recruitment of RAD51 to damage foci in response to the radiomimetic drug neocarzinostatin. We used the widely studied RAD51D-proficient CHO cells (RAD51D.3) and isogenic RAD51D-null cells in which both alleles of RAD51D have been inactivated (RAD51D.1) and complemented these with either a human RAD51D wild-type construct (RAD51D.1-wt) or the c.620C>T;p.S207L variant (RAD51D.1-p.S207L). We found that RAD51D.1 and RAD51D.D1-p.S207L showed a 35.3% and 49.4% decrease in RAD51 focus formation, respectively, compared with wild-type lines Rad51D.3 and RAD51D.1–wt (both P values <0.001; Fig. 2A). This result suggests that RAD51p.S207L may impact HR by impairing RAD51 accumulation at DSBs.

The RAD51D p.S207L mutation prevents DSB repair by HR

To assess the effect of p.S207L in HR-mediated DSB repair, we employed a CRISPR-Cas9–stimulated and HR-mediated gene targeting assay in which the mClover fluorescent protein is inserted at the 5′ end of the Lamin A (LMNA) coding sequence. Using the CHO cell lines previously described, we measured the percentage of mClover-LMNA–positive cells by flow cytometry, which is indicative of functional HR. We observed that the gene targeting frequency remained significantly lower in RAD51D.p.S207L cells compared with RAD51D.1-wt cells ($P < 0.01$; Fig. 2B), further confirming a defect in HR.

Next, we sought to confirm these data in human cells using the direct repeat GFP (DR-GFP) reporter assay. We depleted endogenous RAD51D by siRNA and subsequently expressed ectopically a wild-type mCherry-tagged RAD51D construct or its p.S207L counterpart before inducing DSB in the GFP gene and HR repair. As a control, we used a previously described RAD51D mutant where the Walker B motif was inactivated. We also analyzed the RAD51D-p.E233G variant (rs28363284), as well as a double mutant, p.S207L + p.E233G, to accurately mimic the genotypes seen in our population. Both the RAD51Dp.S207L mutant and the RAD51D-p.S207L + p.E233G double mutant led to a decrease in signal in this assay ($P < 0.01$). Furthermore, the RAD51D-p.E233G variant did not affect DSB repair by HR significantly (Fig. 2C–E). Together, these results unambiguously show that the p.S207L mutation impairs DSB repair by HR, whereas c.698A>G;p.E233G does not.

RAD51D p.S207L abrogates RAD51D–XRCC2 interaction

RAD51D is part of the BCDX2 complex and directly interacts with XRCC2. It was proposed that the functional Walker B domain (amino acids 202–207 in RAD51D) is necessary for the association between RAD51D and XRCC2. As p.S207L localizes to this critical domain, we tested its effect on RAD51D–XRCC2 interaction. As a control, we used the p.D206A mutation, previously shown to abrogate RAD51D–XRCC2 interaction. We expressed Flag-tagged constructs of wild-type RAD51D and its mutants in HEK293T cells and performed an anti-Flag immunoprecipitation. We observed that p.S207L disrupted the RAD51D–XRCC2 interaction in a fashion similar to the previously characterized p.D206A mutation (Fig. 2F; ref. 37). The double mutant p.S207L + p.E233G produced the same phenotype, whereas the p.E233G variant alone had no significant impact on XRCC2 binding.

To better quantify RAD51D–XRCC2 interactions *in vivo*, we used a single-cell assay where we assessed the colocalization, at an integrated lacO array, of an mCherry-tagged LacR-RAD51D fusion protein with endogenous XRCC2. This LacR/lacO system recapitulated the RAD51D–XRCC2 interaction and enabled us to monitor the impact of p.S207L and p.E233G on their association. Although p.E233G alone had only a limited effect, introduction of p.S207L drastically impaired RAD51D–XRCC2 interaction ($P = 7 \times 10^{-9}$). The effect of the p.S207L + p.E233G double mutant was not statistically different from that of p.S207L. Together, these results strongly suggest that RAD51D pS207L impairs HR-mediated DSB repair by disrupting the RAD51D–XRCC2 interaction (Fig. 3A).

RAD51D p.S207L-mutant cells are sensitive to PARP inhibitors

PARP inhibitors (PARPi) elicit apoptosis in RAD51D-deficient cells via synthetic lethality (3). To test the clinically relevant consequences of the p.S207L mutation, we assessed the efficiency of two clinical PARPi [olaparib and talazoparib (BMN 673)] or cisplatin to impair clonogenic survival of cells expressing the RAD51D-620C>T;p.S207L mutant. RAD51D-p.S207L sensitivity to PARPi was then compared with RAD51D-WT, a known benign mutant c.47C>T;p.M16T, RAD51D-null cells and RAD51D-proficient cells (RAD51D.3). As expected, olaparib, talazoparib, or cisplatin reduced clonogenic survival in RAD51D-null cells (RAD51D.1) compared with RAD51D WT cells (RAD51D.3), and RAD51D.1 cells expressing human WT RAD51D or a known benign RAD51D mutant, c.47C>T;p.M16T (ANOVA, $P < 0.0001$, Fig. 3B–E). Talazoparib elicited these effects at lower

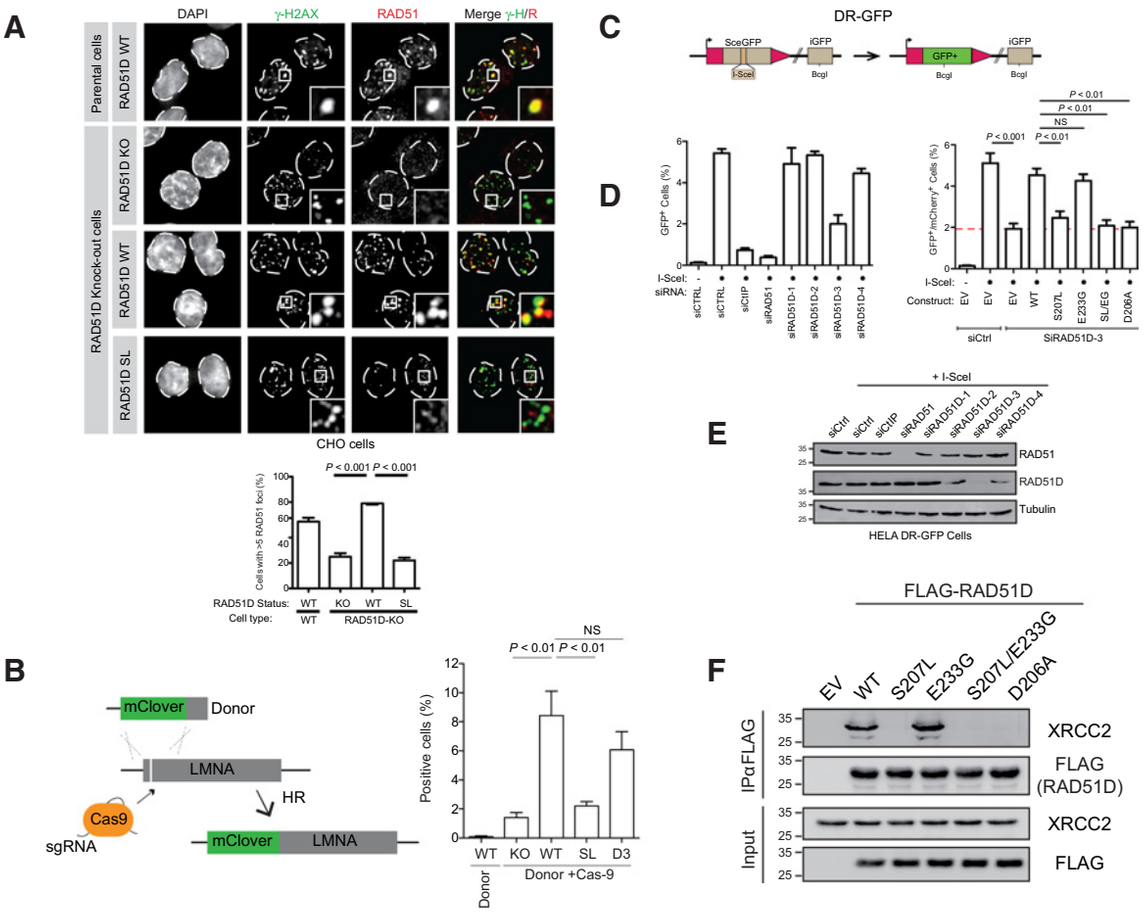

Figure 2.

A, Representative foci formation assay IF micrographs in CHO RAD51D.1-deficient cell line, RAD51D.1-WT, RAD51D.1-p.S207L, and RAD51D.3-proficient cell lines treated with neocarcinostatin (NCS). Immunofluorescence of γH2AX (Alexa 488) was performed in parallel to RAD51 staining (Alexa 647). DAPI, 4′,6-diamidino-2-phenylindole. Graph of the cells with greater than five colocalizing foci and at least 25 cells per cell line were counted. RAD51D SL, RAD51D.1-p.S207L; KO, knockout. Data presented are averages of three independent experiments. Error bars, SDs. *P* values ($P \geq 0.001$) were calculated by ANOVA test, followed by Tukey. **B,** Schematic representation of mClover gene targeting assay and quantification of mClover positives cells (%) in CHO RAD51D.1, RAD51D.1-WT, RAD51D.1-p.S207L, and RAD51D.3 cells. Data presented are averages of three independent experiments. *P* values ($P < 0.01$) were calculated by ANOVA test, followed by Tukey. NS, nonsignificant. **C,** Schema of DR-GFP reporter assay. **D,** Graph of siRNA RAD51D endogenous depletion in HeLa cells and complementation of HR activity in siRNA-resistant mCherry-tagged construct. EV, empty vector; SL/EG = double mutant (p.S207L + E233G); NS, not significant. Data presented are averages of three independent experiments. *P* values were calculated by ANOVA test, followed by Tukey. **E,** Immunoblots of extracts from HELA DR-GFP cells transfected with the indicated siRNAs. CTRL, control. Depletion of endogenous RAD51D was tested with rabbit anti-RAD51D in parallel to endogenous expression of RAD51. TUBB was used as the loading control. **F,** Coimmunoprecipitation (IP) of XRCC2 with FLAG-RAD51D in HEK293T cells. RAD51D expression was probed with anti-Flag clone M2 mouse mAb. XRCC2 Co-IP was checked with mouse anti-XRCC2 antibody. Data presented are averages of three independent experiments.

concentrations than olaparib (Fig. 3B and C), consistent with its enhanced PARP1-trapping abilities (38). RAD51D-null cells expressing the c.620C>T;p.S207L RAD51D mutant were also profoundly sensitive to both PARPi and cisplatin (ANOVA, $P < 0.0001$; Fig. 3B–D), identifying PARPi as a candidate targeted therapy for *RAD51D* c.620C>T;p.S207L carriers.

Discussion

The maintenance of genome integrity is fundamental for cancer biology and is of clinical importance. This past decade, rapid advances in genomics have accelerated the discovery of critical players in this process and the establishment of genetic screening programs for high-risk individuals. In this study, we provide new insight into the functions of RAD51D and demonstrated that (i) the *RAD51D* variant 620C>T;p.S207L destabilizes the RAD51D–XRCC2 binding, resulting in impaired HR and (ii) this variant predisposes to ovarian cancer. Although this work is seminal in better understanding RAD51D in the maintenance of genome stability and ovarian cancer predisposition, it also provides new insight into the FC population as c.620C>T is a founder variant.

More than a decade after the discovery of *BRCA1/2*, likely truncating variants in *RAD51C* and *RAD51D* paralogs were associated with susceptibility to ovarian cancer (3, 39, 40). Loveday and colleagues (3) reported the presence of *RAD51D* missense variants at similar frequency in cases and controls and argued that

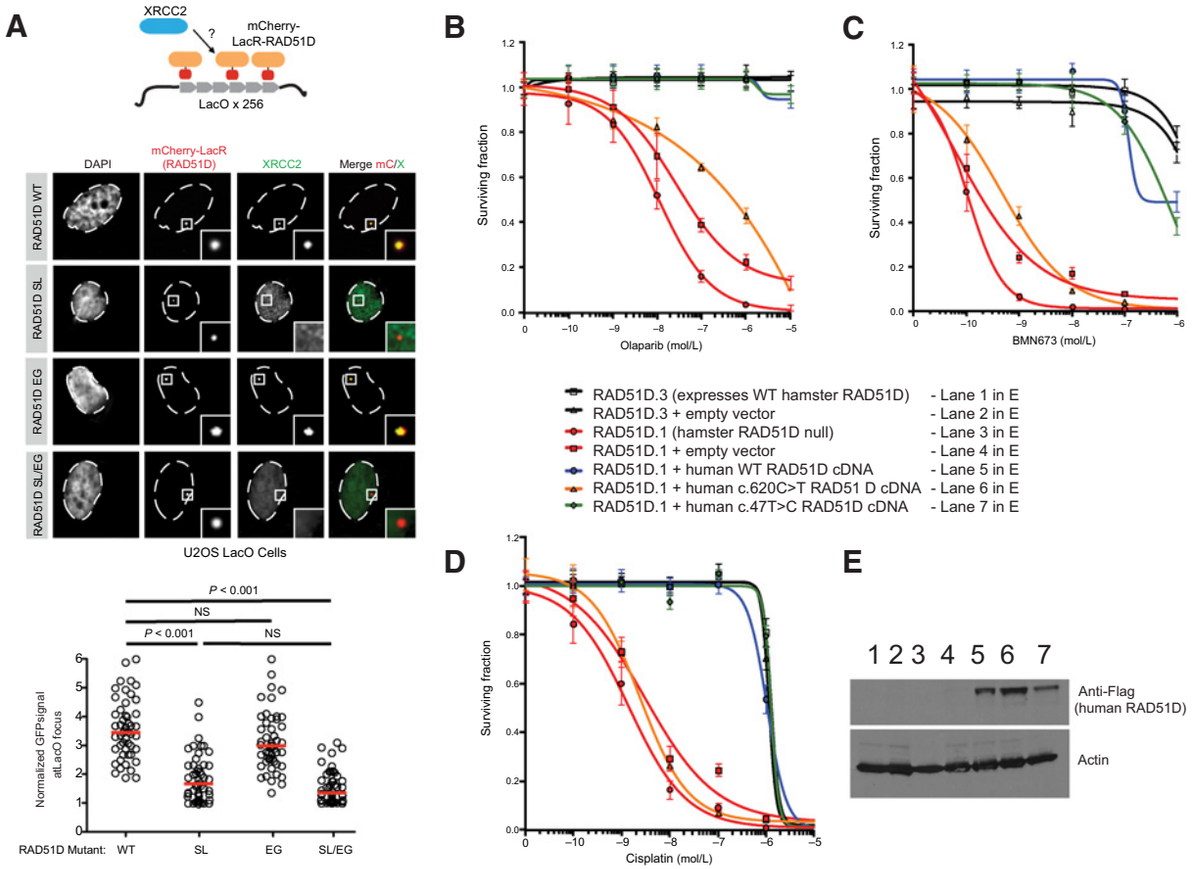

Figure 3.

A, Representative micrograph and quantitative assessment of the RAD51D–XRCC2 interaction *in vivo* in U2OS LacO cells transfected with LacR-tagged constructs. EV, empty vector; SL/EG, double mutant (p.S207L + E233G); data presented are averages of three independent experiments, and at least 50 cells were counted per cell line. $P < 0.001$; ANOVA test, followed by Tukey. NS, not significant. **B–D,** Clonogenic survival assays of CHO RAD51D.1 (RAD51D null) and RAD51D.3 (RAD51D WT) cells expressing WT or mutant forms of human RAD51D, exposed to olaparib (**B**), talazoparib (**C**), and cisplatin (**D**) for 7 days. Error bars, SEM from three replica experiments. ANOVA ($P < 0.0001$) RAD51D.1, RAD51D.1 + empty, and RAD51D.1 c.620C>T;p.S207L cells versus other conditions. **E,** Western blot analysis showing stable expression of human RAD51D in RAD51D.1 cells. Human RAD51D expression detected using anti-Flag clone M2 mouse mAb.

missense variants of the gene were unlikely to be damaging. Contrary to this hypothesis, we conclusively demonstrate the deleterious effects of a missense variant in *RAD51D*. Our study show that the c.620C>T;p.S207L missense variant is clearly pathogenic; it is one of the most frequently observed alleles conferring high risk of ovarian HGSC in the FC population of Quebec (Supplementary Table S4) and is similar in frequency to other prevalent variants associated with increased ovarian cancer risk in founder populations of European ancestry reviewed in 2010 (41).

The presence of somatic mutations in the *TP53* gene is a well-known feature of HGSC; more recently, the ability to compile the entire repertoire of somatic events occurring in a tumor has led to the description of mutational signatures that reflect the type of mutations predominant in a tumor and provide clues about the mechanisms involved in their generation. Molecular signature 3 characterizes HR-deficient tumors, is highly associated to *BRCA1/2* mutations, and is known to be prevalent in ovarian HGSC (36). After confirming the presence of somatic mutations in *TP53* in all tumors from carriers, we further verified the predominance of signature 3 and a complex pattern of chromosomal aberrations throughout the genome, all landmark features of a deficiency in HR. Somatically, no pathogenic mutations in DNA repair genes were found in the tumors except for a unique heterozygous missense variant in *FANCB* (Supplementary Table S2). These findings reinforced our premise that c.620C>T;p.S207L is the main driver of HR deficiency seen in these tumors and confirmed the relevance of functionally investigating the consequences of this mutation on HR repair efficiency. Furthermore, these results further support that the mutational signature 3 in *BRCA1/2* wild-type tumors might be prompted by mutations in other HR genes as hypothesized previously (36, 42), advocating for the suitability of comprehensive genomic landscape profiling as a predictor for PARP therapy responsiveness.

Although the biochemical functions of the RAD51 paralogs are not all well understood, the HR process is clearly a dynamic process that requires enough plasticity to favor multiprotein complex rearrangements and allow the recruitment of RAD51 to the DSB. The latter ensures a proper interaction between paralogs as well as between protein and DNA (43). The kinetics of these interactions rely upon the ATPase activity of the conserved Walker

A and B domains. Specifically, the integrity of a functional Walker B domain of RAD51D was reported to be essential for RAD51D–XRCC2 and RAD51C complex formation (37). We uncover a deleterious effect of c.620C>T;p.S207L on RAD51D HR activity where the key event is disruption of the interaction between RAD51D and XRCC2 paralogs of RAD51, both essential for RAD51 recruitment to DSBs upon DNA damage. This mechanism combined with the drastic effect that PARPi exhibited in the viability of c.620C>T;p.S207L-RAD51D cells further supports the notion that PARPi-targeted therapy will likely be effective in c.620C>T;p.S207L carriers. In addition, acquired resistance to PARPi in TNBC has recently been associated with RAD51 proficiency (44). Furthermore, the current study highlights the central importance of the RAD51D–XRCC2 interaction as a driver mechanism for tumorigenesis and consequently the pathogenicity likelihood of other deleterious missense mutations mapping within the Walker B domain of RAD51D.

The role of *RAD51D* mutations in breast cancer risk remains unresolved (3, 4, 45, 46), and a possible involvement of *RAD51D* specifically in TNBC seems plausible (47). Our results do not support an association between c.620C>T;p.S207L and breast cancer in FCs although our study has limited power to rule out such an association. The p.E233G (rs28363284) variant was previously studied in the context of breast cancer–associated risk, then functionally, but its association with breast cancer risk remains controversial (48), and its high frequency in public databases suggests it is a benign variant. In 2009, two studies from the same group described increased resistance by p.E233G to DNA-damaging agents upon p53 abrogation (49). However, our results show that p.E233G can restore DNA repair ability in RAD51D-depleted cells where p53 is present, suggesting therefore that p.E233G does not diminish RAD51D HR activity by itself.

The implications of this single mutation contributing to almost 4% of all ovarian HGSC in a founder population are significant and justify the need to establish surveillance and management programs for individuals at risk. Nowadays, with personalized health care as a global aim, there is open debate regarding the suitability of genetic testing at the population level, with different models under consideration. Population-specific approaches have their supporters (50), and this study certainly suggests that widespread testing of the FC population of Quebec for this and other founder variants could be an efficient, cost-effective approach to lessen the burden of cancer.

Disclosure of Potential Conflicts of Interest

No potential conflicts of interest were disclosed.

Authors' Contributions

Conception and design: B. Rivera, R. Siebert, P.N. Tonin, A. Orthwein, W.D. Foulkes

Development of methodology: B. Rivera, M. Di Iorio, S.L. Arcand, P.N. Tonin, A. Orthwein

Acquisition of data (provided animals, acquired and managed patients, provided facilities, etc.): B. Rivera, M. Di Iorio, J. Frankum, S.L. Arcand, D. Grapton, E. Tomiak, V. Hastings, N. Hamel, R. Wagener, F.F. Hamdan, A. Dionne-Laporte, G. Zogopoulos, F. Rousseau, D. Provencher, G.A. Rouleau, J.L. Michaud, A.-M. Mes-Masson, S. Bens, S.A. Narod, M.R. Akbari, C.J. Lord, P.N. Tonin, A. Orthwein, W.D. Foulkes

Analysis and interpretation of data (e.g., statistical analysis, biostatistics, computational analysis): B. Rivera, M. Di Iorio, J. Frankum, J. Nadaf, S. Fahiminiya, S.L. Arcand, D.L. Burk, N. Hamel, R. Wagener, A.M. Berghuis, J.L. Michaud, J. Majewski, S. Bens, R. Siebert, C.J. Lord, P.N. Tonin, A. Orthwein, W.D. Foulkes

Writing, review, and/or revision of the manuscript: B. Rivera, M. Di Iorio, J. Nadaf, S. Fahiminiya, E. Tomiak, N. Hamel, R. Wagener, F.F. Hamdan, A. Dionne-Laporte, G. Zogopoulos, F. Rousseau, A.M. Berghuis, G.A. Rouleau, A.-M. Mes-Masson, S. Bens, R. Siebert, M.R. Akbari, P.N. Tonin, A. Orthwein, W.D. Foulkes

Administrative, technical, or material support (i.e., reporting or organizing data, constructing databases): B. Rivera, R. Wagener, O. Aleynikova, S. Bens, P.N. Tonin, W.D. Foulkes

Study supervision: R. Siebert, P.N. Tonin, W.D. Foulkes

Other (identified and prepared colorectal cases and extracted DNA from FFPE samples): S. Giroux

Acknowledgments

We thank D. Durocher for plasmids/cell lines, A.C. Gingras for pDEST constructs, J. Stark for U2OS DR-GFP cells, R. Greenberg for U2OS LacO cells, and G. Dellaire for CRISPR/Cas9 LMNA plasmids. We thank Jian Zhang for her initial work on this project, Laura Palma CGC for clinical care of the index family, Nelly Sabbaghian, Eric Bareke, Lilian Amrein, Manon de Ladurantaye, Lise Portelance, Pablo Gonzalez-Ginestet, and Alyssa Smith and the technicians of the molecular cytogenetic laboratory in Ulm, Germany, for technical support.

Grant Support

This work was financed in part by research grants to W.D. Foulkes from the Quebec Breast Cancer Foundation, Susan G. Komen, and the Canadian Institutes of Health Research (CIHR; FDN-148390) and a CIHR Project grant to A. Orthwein (361708). This work was supported in part by grants to P.N. Tonin from the Cancer Research Society of Canada and Fonds de recherche du Québec-Santé (FRQS). Tumor banking was supported by the Banque de tissus et données of the Réseau de recherche sur le cancer of the Fond de Recherche du Québec - Santé (FRQS), associated with the Canadian Tumor Repository Network (CTRNet). A. Orthwein also receives a Transition Grant from the Cole Foundation and is supported by the Sir Mortimer B. Davis Foundation from the Jewish General Hospital. B. Rivera was a fellow of Fundacion Martin Escudero international postdoctoral fellowship program and FQRNT- Quebec Merit Scholarship. M.R. Di Iorio was recipient of an MICRTP studentship program and the Dr. Clarke K. McLeod Memorial Scholarship. M.R. Akbari was supported by Canadian Cancer Society Research Institute. C.J. Lord receives funding from Cancer Research UK. F. Rousseau holds a salary award from the FRQ-Santé in evidence-based laboratory medicine. The Research Institute of the McGill University Health Centre and the Centre de recherche du Centre Hospitalier de l'Université de Montréal receive grant support from the FRQS.

The costs of publication of this article were defrayed in part by the payment of page charges. This article must therefore be hereby marked *advertisement* in accordance with 18 U.S.C. Section 1734 solely to indicate this fact.

Received January 24, 2017; revised March 23, 2017; accepted June 6, 2017; published OnlineFirst June 23, 2017.

References

1. Constantinou P, Tischkowitz M. Genetics of gynaecological cancers. Best Pract Res Clin Obstet Gynaecol 2017 Jan 24. [Epub ahead of print].
2. Nielsen FC, van Overeem Hansen T, Sorensen CS. Hereditary breast and ovarian cancer: new genes in confined pathways. Nat Rev Cancer 2016;16:599–612.
3. Loveday C, Turnbull C, Ramsay E, Hughes D, Ruark E, Frankum JR, et al. Germline mutations in RAD51D confer susceptibility to ovarian cancer. Nat Genet 2011;43:879–82.
4. Osher DJ, De Leeneer K, Michils G, Hamel N, Tomiak E, Poppe B, et al. Mutation analysis of RAD51D in non-BRCA1/2 ovarian and breast cancer families. Br J Cancer 2012;106:1460–3.
5. Wickramanayake A, Bernier G, Pennil C, Casadei S, Agnew KJ, Stray SM, et al. Loss of function germline mutations in RAD51D in women with ovarian carcinoma. Gynecol Oncol 2012;127:552–5.
6. Song H, Dicks E, Ramus SJ, Tyrer JP, Intermaggio MP, Hayward J, et al. Contribution of germline mutations in the RAD51B, RAD51C, and

RAD51D genes to ovarian cancer in the population. J Clin Oncol 2015;33:2901–7.
7. Manolio TA, Collins FS, Cox NJ, Goldstein DB, Hindorff LA, Hunter DJ, et al. Finding the missing heritability of complex diseases. Nature 2009;461:747–53.
8. Spurdle AB, Healey S, Devereau A, Hogervorst FB, Monteiro AN, Nathanson KL, et al. ENIGMA–evidence-based network for the interpretation of germline mutant alleles: an international initiative to evaluate risk and clinical significance associated with sequence variation in BRCA1 and BRCA2 genes. Hum Mutat 2012;33:2–7.
9. Lindor NM, Guidugli L, Wang X, Vallee MP, Monteiro AN, Tavtigian S, et al. A review of a multifactorial probability-based model for classification of BRCA1 and BRCA2 variants of uncertain significance (VUS). Hum Mutat 2012;33:8–21.
10. Couch FJ, Rasmussen LJ, Hofstra R, Monteiro AN, Greenblatt MS, de Wind N, et al. Assessment of functional effects of unclassified genetic variants. Hum Mutat 2008;29:1314–26.
11. Millot GA, Carvalho MA, Caputo SM, Vreeswijk MP, Brown MA, Webb M, et al. A guide for functional analysis of BRCA1 variants of uncertain significance. Hum Mutat 2012;33:1526–37.
12. Shimelis H, Mesman RL, Von Nicolai C, Ehlen A, Guidugli L, Martin C, et al. BRCA2 hypomorphic missense variants confer moderate risks of breast cancer. Cancer Res 2017;77:2789–99.
13. Ghadirian P, Robidoux A, Zhang P, Royer R, Akbari M, Zhang S, et al. The contribution of founder mutations to early-onset breast cancer in French-Canadian women. Clin Genet 2009;76:421–6.
14. Cybulski C, Carrot-Zhang J, Kluzniak W, Rivera B, Kashyap A, Wokolorczyk D, et al. Germline RECQL mutations are associated with breast cancer susceptibility. Nat Genet 2015;47:643–6.
15. Belanger MH, Dolman L, Arcand SL, Shen Z, Chong G, Mes-Masson AM, et al. A targeted analysis identifies a high frequency of BRCA1 and BRCA2 mutation carriers in women with ovarian cancer from a founder population. J Ovarian Res 2015;8:1.
16. Kotar KV, Osczevski K, Yamani L, Galvez M, Hamel N, Ferrara E, et al. One of six founder mutations account for nearly 75% of all BRCA1/2 mutations in French Canadian women attending two McGill University high-risk clinics. In: Proceedings of the 2005 American Society of Human Genetics Annual Meeting; 2005 Oct 25–29; Salt Lake City, UT. Bethesda, MD: ASHG; 2005.
17. Liu G, Ghadirian P, Vesprini D, Hamel N, Paradis AJ, Lal G, et al. Polymorphisms in GSTM1, GSTT1 and CYP1A1 and risk of pancreatic adenocarcinoma. Br J Cancer 2000;82:1646–9.
18. Castellsague E, Liu J, Volenik A, Giroux S, Gagne R, Maranda B, et al. Characterization of a novel founder MSH6 mutation causing Lynch syndrome in the French Canadian population. Clin Genet 2015;87:536–42.
19. Ancot F, Arcand SL, Mes-Masson AM, Provencher DM, Tonin PN. Double PALB2 and BRCA1/BRCA2 mutation carriers are rare in breast cancer and breast-ovarian cancer syndrome families from the French Canadian founder population. Oncol Lett 2015;9:2787–90.
20. Rudkin TM, Hamel N, Galvez M, Hogervorst F, Gille JJ, Moller P, et al. The frequent BRCA1 mutation 1135insA has multiple origins: a haplotype study in different populations. BMC Med Genet 2006;7:15.
21. Fahiminiya S, Witkowski L, Nadaf J, Carrot-Zhang J, Goudie C, Hasselblatt M, et al. Molecular analyses reveal close similarities between small cell carcinoma of the ovary, hypercalcemic type and atypical teratoid/rhabdoid tumor. Oncotarget 2016;7:1732–40.
22. McKenna A, Hanna M, Banks E, Sivachenko A, Cibulskis K, Kernytsky A, et al. The Genome Analysis Toolkit: a MapReduce framework for analyzing next-generation DNA sequencing data. Genome Res 2010;20:1297–303.
23. Wang K, Li M, Hakonarson H. ANNOVAR: functional annotation of genetic variants from high-throughput sequencing data. Nucleic Acids Res 2010;38:e164.
24. Robinson JT, Thorvaldsdottir H, Winckler W, Guttman M, Lander ES, Getz G, et al. Integrative genomics viewer. Nat Biotechnol 2011;29:24–6.
25. Chae YK, Anker JF, Carneiro BA, Chandra S, Kaplan J, Kalyan A, et al. Genomic landscape of DNA repair genes in cancer. Oncotarget 2016;7:23312–21.
26. Nadaf J, Majewski J, Fahiminiya S. ExomeAI: detection of recurrent allelic imbalance in tumors using whole-exome sequencing data. Bioinformatics 2015;31:429–31.
27. Alexandrov LB, Nik-Zainal S, Siu HC, Leung SY, Stratton MR. A mutational signature in gastric cancer suggests therapeutic strategies. Nat Commun 2015;6:8683.
28. Wojnarowicz PM, Oros KK, Quinn MC, Arcand SL, Gambaro K, Madore J, et al. The genomic landscape of TP53 and p53 annotated high grade ovarian serous carcinomas from a defined founder population associated with patient outcome. PLoS One 2012;7:e45484.
29. Ventura RA, Martin-Subero JI, Jones M, McParland J, Gesk S, Mason DY, et al. FISH analysis for the detection of lymphoma-associated chromosomal abnormalities in routine paraffin-embedded tissue. J Mol Diagn 2006;8:141–51.
30. Kelley LA, Mezulis S, Yates CM, Wass MN, Sternberg MJ. The Phyre2 web portal for protein modeling, prediction and analysis. Nat Protoc 2015;10:845–58.
31. Schrodinger LLC. The PyMOL Molecular Graphics System, Version 1.8. 2015.
32. Hinz JM, Tebbs RS, Wilson PF, Nham PB, Salazar EP, Nagasawa H, et al. Repression of mutagenesis by Rad51D-mediated homologous recombination. Nucleic Acids Res 2006;34:1358–68.
33. Pinder J, Salsman J, Dellaire G. Nuclear domain `knock-in' screen for the evaluation and identification of small molecule enhancers of CRISPR-based genome editing. Nucleic Acids Res 2015;43:9379–92.
34. Orthwein A, Noordermeer SM, Wilson MD, Landry S, Enchev RI, Sherker A, et al. A mechanism for the suppression of homologous recombination in G1 cells. Nature 2015;528:422–6.
35. Lek M, Karczewski KJ, Minikel EV, Samocha KE, Banks E, Fennell T, et al. Analysis of protein-coding genetic variation in 60,706 humans. Nature 2016;536:285–91.
36. Alexandrov LB, Nik-Zainal S, Wedge DC, Aparicio SA, Behjati S, Biankin AV, et al. Signatures of mutational processes in human cancer. Nature 2013;500:415–21.
37. Wiese C, Hinz JM, Tebbs RS, Nham PB, Urbin SS, Collins DW, et al. Disparate requirements for the Walker A and B ATPase motifs of human RAD51D in homologous recombination. Nucleic Acids Res 2006;34:2833–43.
38. Murai J, Huang SY, Renaud A, Zhang Y, Ji J, Takeda S, et al. Stereospecific PARP trapping by BMN 673 and comparison with olaparib and rucaparib. Mol Cancer Ther 2014;13:433–43.
39. Loveday C, Turnbull C, Ruark E, Xicola RM, Ramsay E, Hughes D, et al. Germline RAD51C mutations confer susceptibility to ovarian cancer. Nat Genet 2012;44:475–6.
40. Meindl A, Hellebrand H, Wiek C, Erven V, Wappenschmidt B, Niederacher D, et al. Germline mutations in breast and ovarian cancer pedigrees establish RAD51C as a human cancer susceptibility gene. Nat Genet 2010;42:410–4.
41. Janavicius R. Founder BRCA1/2 mutations in the Europe: implications for hereditary breast-ovarian cancer prevention and control. EPMA J 2010;1:397–412.
42. Nik-Zainal S, Davies H, Staaf J, Ramakrishna M, Glodzik D, Zou X, et al. Landscape of somatic mutations in 560 breast cancer whole-genome sequences. Nature 2016;534:47–54.
43. Suwaki N, Klare K, Tarsounas M. RAD51 paralogs: roles in DNA damage signalling, recombinational repair and tumorigenesis. Semin Cell Dev Biol 2011;22:898–905.
44. Liu Y, Burness ML, Martin-Trevino R, Guy J, Bai S, Harouaka R, et al. RAD51 mediates resistance of cancer stem cells to PARP inhibition in triple-negative breast cancer. Clin Cancer Res 2017;23:514–22.
45. Baker JL, Schwab RB, Wallace AM, Madlensky L. Breast cancer in a RAD51D mutation carrier: case report and review of the literature. Clin Breast Cancer 2015;15:e71–5.
46. Gutierrez-Enriquez S, Bonache S, de Garibay GR, Osorio A, Santamarina M, Ramon y Cajal T, et al. About 1% of the breast and ovarian Spanish families testing negative for BRCA1 and BRCA2 are carriers of RAD51D pathogenic variants. Int J Cancer 2014;134:2088–97.
47. Couch FJ, Hart SN, Sharma P, Toland AE, Wang X, Miron P, et al. Inherited mutations in 17 breast cancer susceptibility genes among a large

triple-negative breast cancer cohort unselected for family history of breast cancer. J Clin Oncol 2015;33:304–11.
48. Dowty JG, Lose F, Jenkins MA, Chang JH, Chen X, Beesley J, et al. The RAD51D E233G variant and breast cancer risk: population-based and clinic-based family studies of Australian women. Breast Cancer Res Treat 2008;112:35–9.
49. Nadkarni A, Rajesh P, Ruch RJ, Pittman DL. Cisplatin resistance conferred by the RAD51D (E233G) genetic variant is dependent upon p53 status in human breast carcinoma cell lines. Mol Carcinog 2009;48:586–91.
50. Foulkes WD, Knoppers BM, Turnbull C. Population genetic testing for cancer susceptibility: founder mutations to genomes. Nat Rev Clin Oncol 2016;13:41–54.